Chemical Science

ROYAL SOCIETY OF CHEMISTRY

EDGE ARTICLE

View Article Online
View Journal

Cite this: DOI: 10.1039/d6sc00730a

All publication charges for this article have been paid for by the Royal Society of Chemistry

Enzymatically hydrolyzed oligosaccharide fingerprinting using nanopipettes at the single-molecule level

Qi-Yun Lu,†[a] Hui Ma †*[b] and Shi-Guo Chen *[a]

Enzymatic hydrolysis of oligosaccharides plays a pivotal role in important biological processes, but conventional analytical tools struggle to determine these functional components with single-monosaccharide resolution and ultrahigh sensitivity. Here, we report a nanopipette-based strategy for the length discrimination of enzymatically hydrolyzed galacturonic acid oligosaccharides differing by a single monosaccharide unit while achieving femtomolar (fM) level detection limits. Using this approach, we precisely identify six types of enzymatic hydrolysates, even in complex mixtures. Incorporating machine learning further enhances classification performance, achieving 0.98 accuracy. This study establishes an advanced platform for high-precision carbohydrate analysis, offering new possibilities for glycosidase-assisted glycan sequencing, enzymatic degradation studies, and gut microbiota metabolism research.

Received 26th January 2026
Accepted 16th May 2026

DOI: 10.1039/d6sc00730a

rsc.li/chemical-science

Introduction

Enzymatic hydrolysis of polysaccharides generates oligosaccharides with structural characteristics that play critical roles in nutrition,[1] and biological regulation.[2] However, the precise analysis of these hydrolysates is inherently challenging because of their trace amounts in complex biological samples and their high structural similarity, where species may differ by only a single monosaccharide residue.[3] Such subtle variations can profoundly affect molecular recognition and biological activity.[4] This challenge is further compounded by the fact that many bioactive oligosaccharides exist at ultra-trace concentrations (fM–nM) in biological systems, where they can cross the intestinal barrier and exert systemic effects.[5,6] Current analytical techniques, such as nuclear magnetic resonance (NMR) spectroscopy[7,8] and mass spectrometry (MS),[9,10] have provided significant insights into polysaccharide structures. However, their use is constrained by labor-intensive procedures and limited sensitivity toward low-abundance species.[8,11] For example, NMR and MS require sample concentrations well above 0.01% by mass (nM–μM),[12–14] necessitating μg-scale samples, which are often impractical for detecting trace-level oligosaccharides within complex biological systems. Given these limitations, there is an urgent need for ultra-sensitive analytical technologies that can detect and structurally profile oligosaccharides at trace levels, including those generated by enzymatic hydrolysis. Such advancements would enable deeper insights into glycan function and offer new opportunities for precise regulation of their biological effects.

Nanopore-based sensing offers a promising alternative, enabling single-molecule detection of oligosaccharides through their characteristic ionic current signatures.[15] While engineered biological nanopores can distinguish oligosaccharide building blocks and chain lengths,[16–18] they generally require high concentrations (*e.g.*, 10–500 μM),[19–21] limiting their applicability in biological and clinical samples where glycans are often present at much lower concentrations. In contrast, nanopipettes offer detection limits in the femtomolar (fM) to picomolar (pM) range.[22–25] However, their application to small oligosaccharides has been hindered by rapid translocation speeds and limited spatial resolution,[26–28] due to the relatively large pore sizes that impede reliable discrimination at the single-saccharide level.[29,30]

Here, we demonstrate a proof-of-concept for length-discrimination of enzymatically hydrolyzed galacturonic acid oligosaccharides using nanopipettes. As representative acidic glycans with indicative bioactivity but poorly defined biological roles,[31,32] their strong anionic nature often complicates their detection. Our method distinguishes oligosaccharides with length differences of a single monosaccharide unit either independently or in mixtures. It achieves exceptional sensitivity, detecting galacturonic acid oligosaccharides down to 1 fM (using ~200 μL sample volume), a concentration 10^6–10^9 times

[a]College of Biosystems Engineering and Food Science, National-Local Joint Engineering Laboratory of Intelligent Food Technology and Equipment, Zhejiang Key Laboratory of Edible Agricultural Resources and High-value Utilization Zhejiang Key Laboratory for Agro-Food Processing, Zhejiang Engineering Laboratory of Food Technology and Equipment, Zhejiang University, Hangzhou 310058, P.R. China. E-mail: chenshiguo210@163.com

[b]School of Chemistry and Chemical Engineering, Zhejiang Sci-Tech University, Hangzhou, 310038, P.R. China. E-mail: huima@zstu.edu.cn

† These authors contributed equally to this work.

lower than current MS and NMR detection limits.[33,34] With machine learning, we further discriminate six distinct oligosaccharides with an accuracy of 0.98. These results highlight the potential of nanopipette technology to achieve single-oligosaccharide length discrimination and sequence recognition for trace enzymatic hydrolysis products. This advancement opens up new possibilities in nutrition, microbiome analysis, and therapeutics.

Results and discussion

A library of enzymatically derived oligosaccharides was prepared by treating high-molecular-weight polygalacturonic acid (average M_W ~150 kDa) with controlled demethylation followed by glycosidase hydrolysis (SI Method, Fig. S1–S4, and Tables S1 and S2). This process selectively cleaved glycosidic bonds, yielding oligosaccharides of defined chain lengths. The resulting hydrolysates were purified in two steps: size-exclusion chromatography to enrich lower-molecular-weight fractions and hydrophilic interaction liquid chromatography (HILIC) separation for further refinement (Fig. S5 and S6). Mass spectrometry analysis (Fig. S7–S9) confirmed the sequential increase in the degree of polymerization (DP) among the purified oligosaccharides (GalA2-6).[35]

This well-defined oligosaccharide library was then used as analytical standards to establish a nanopipette-based sensing platform (Fig. 1). To achieve robust detection, nanopipettes with various diameters were evaluated. A 13 nm pore exhibited a higher signal-to-noise ratio (SNR) and greater event efficiency for oligosaccharide GalA5 (the oligosaccharide with the smallest current blockades among the tested oligosaccharides) compared to a 40 nm pore (Fig. S10). Consequently, 13 nm nanopipettes were therefore selected for all subsequent experiments. The measurements were conducted in 0.2 M phosphate buffer (PB) containing 200 pM glycerol at pH 7.4 under a continuously applied potential of +600 mV, unless otherwise specified. The resulting ionic current rectification ratio falls within the optimal range of 2.0 ± 0.4 (Fig. S11 and S12). Notably, the enzymatically generated oligosaccharides carried net negative charges.[36] The oligosaccharides were primarily driven by electrophoretic force (EPF) toward the pore, with a weak counteracting electroosmotic flow (EOF) enabling controlled passage through the pore.[37,38] This optimized system provided a high event frequency and high SNR (Table S3). The selection of these specific buffer conditions was validated through control experiments. At higher ionic strengths (1 M PB), a reduced EOF led to rapid movement of oligosaccharides, decreasing both the event frequency and current blockade amplitude (Fig. S13). Under lower ionic strength conditions (0.02 M PB), a stronger EOF hindered analyte entry into the nanopipette, and no current blockades were recorded. At pH 7.4, the rectification ratio remained within an appropriate range (Fig. S14), generating signals with a high SNR that enable discrimination of single oligosaccharide molecules. In addition, this condition preserved the structural integrity of the oligosaccharides.

Six galacturonic acid oligosaccharides (GalA1-6) at a final concentration of 10 fM were analyzed using nanopipettes to characterize the enzymatic products at the single-molecule level. All oligosaccharides generated distinct characteristic

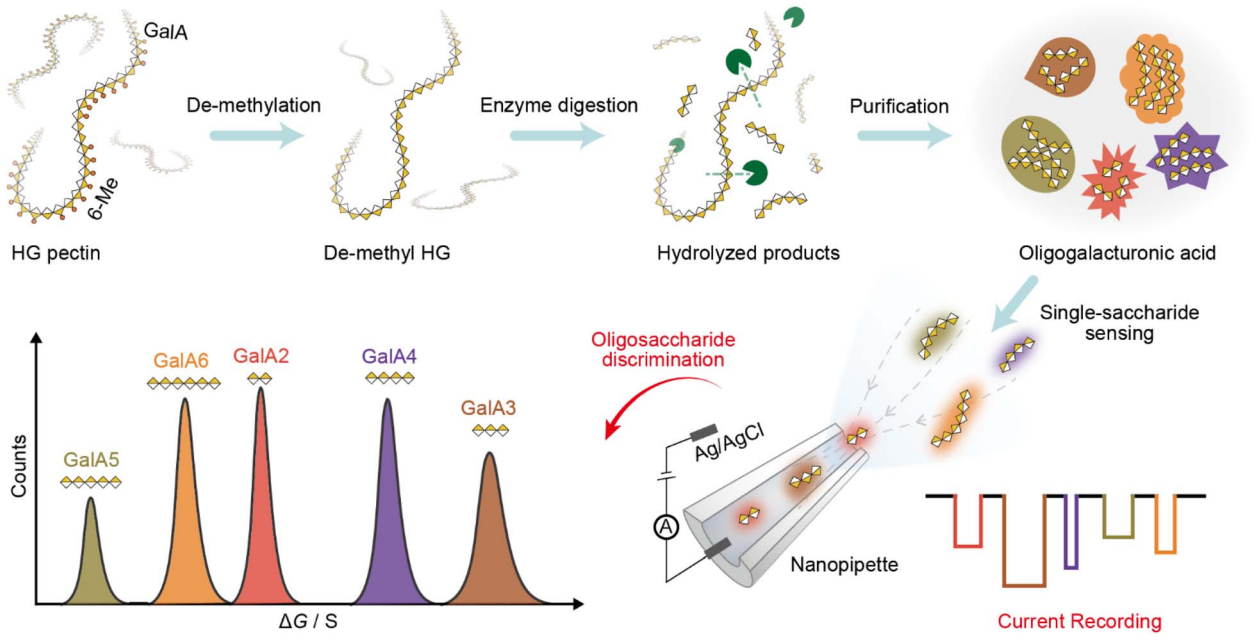

Fig. 1 Schematic workflow for the preparation of enzymatically hydrolyzed oligosaccharides and nanopore reading using a nanopipette. Commercial homogalacturonan was demethylesterified, enzymatically hydrolyzed by endo-polygalacturonase, and purified using Superdex HiLoad and XAmide chromatography. Oligosaccharides with varying polymerization degrees were individually measured using a nanopipette, revealing distinct current signals based on conductance characteristics.

current blockades under a positive applied voltage, demonstrating a high capture rate (Fig. 2a–f). Scatter plots from six independent datasets showed well-separated clusters for each species, with ΔG serving as the primary discriminator (Fig. 2g). GalA5, a higher-degree-of-polymerization fragment from enzymatic hydrolysis, produced the smallest ΔG, indicating minimal current blockade, while its dwell time remained considerable. GalA5 and GalA6 were clearly

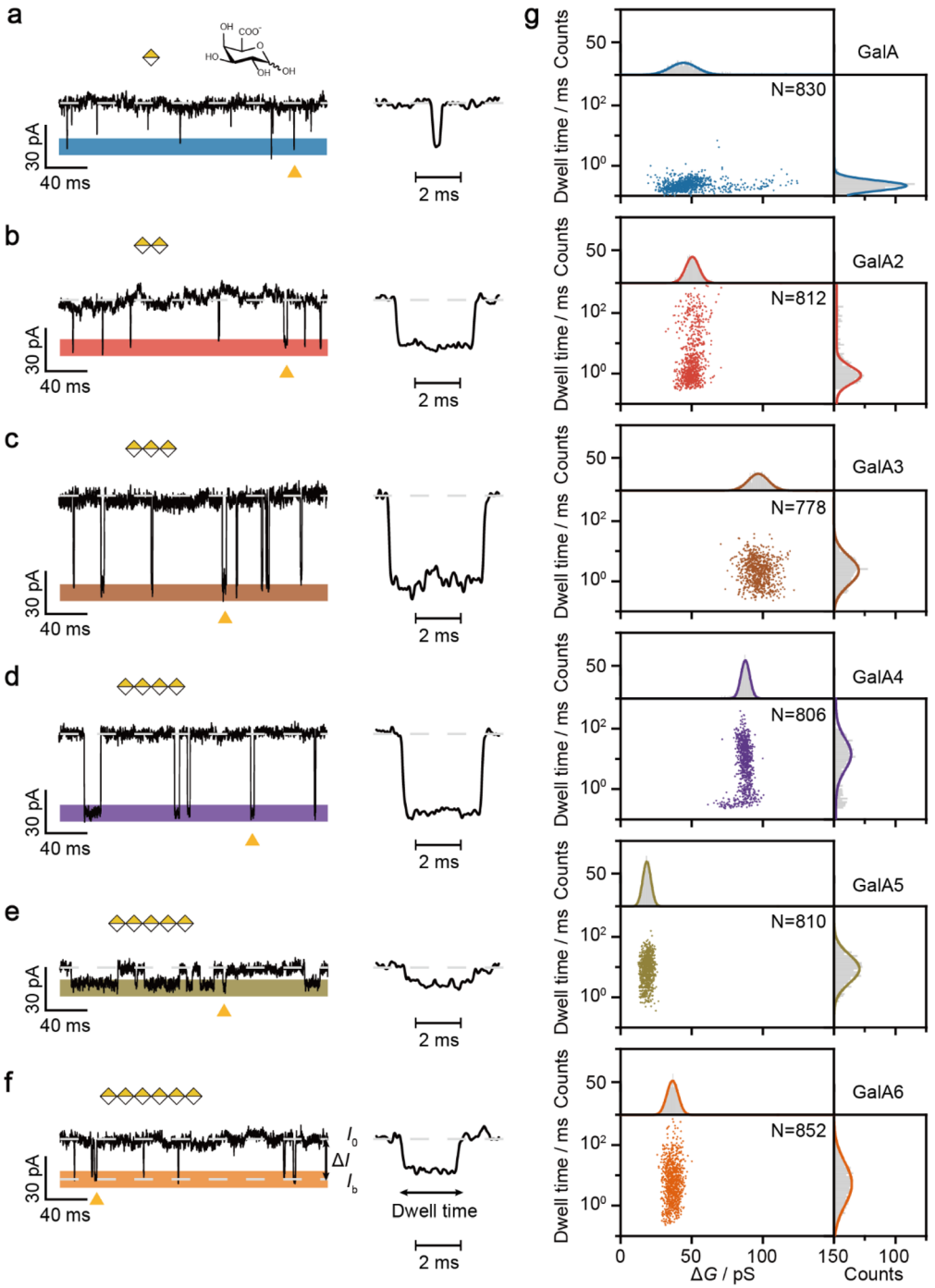

Fig. 2 Identification of galacturonic acid oligosaccharides using nanopipettes. (a–f) Symbol Nomenclature for Glycans (SNFG) representations of GalA1-6 and their corresponding characteristic current signals. All measurements were performed in 0.2 M PB solution (pH 7.4) containing 200 pM glycerol at +600 mV, with each oligosaccharide (GalA: blue, GalA2: red, GalA3: brown, GalA4: purple, GalA5: green, and GalA6: orange). Each sample was individually added to the cis chamber with a final concentration of 10 fM. The open pore current (I_0) and the mean value of blockage current (I_b) were marked in gray dashed lines. ΔG was calculated as ΔI divided by applied voltage. (g) Scatter plot of ΔG (pS) against the logarithmic form of dwell time (ms) and corresponding histogram (bin size = 0.6 for ΔG and bin size = 0.06 for dwell time) from six independent experiments. Sensing events for each type of galacturonic acid oligosaccharide were labeled with different colors.

discriminated based on their conductance blockades, in agreement with mass spectrometric identification of the two species as distinct parent ions (Fig. S9). Even the smallest commercially obtained sample, GalA, produced well-defined translocation events, characterized by extremely short dwell times and sharp current spikes (Fig. 2a).

Among the analyzed oligosaccharides, GalA3 exhibited the largest conductance blockade (85–110 pS) and a relatively broader distribution compared with other oligosaccharides. In comparison, GalA4 produced conductance blockade amplitudes in the range of 78–92 pS, with a distribution slightly shifted to lower values relative to GalA3. Overall, the oligosaccharides generated characteristic ionic current signatures that enabled their discrimination at the single-molecule level. Note that the ΔG of oligosaccharides does not strictly correlate with molecular size. Interactions with the nanopore may also contribute to the ionic current blockade, although the specific mechanism requires further investigation.

We next evaluated the quantitative performance of the nanopipette by analyzing GalA6 across concentrations from 1 fM to 100 fM (Fig. 3a), a representative molecule commonly used in functional studies.[39] Characteristic current blockades remained readily detectable even at 1 fM, with characteristic amplitudes that remained consistent across the concentration range (Fig. 3b and S15). Event frequency scaled linearly with analyte concentration (Fig. 3c), consistent with a diffusion-limited capture process.[40,41] These results demonstrate that nanopipettes offer both high sensitivity and high resolution for structural profiling of oligosaccharides even at fM concentrations.

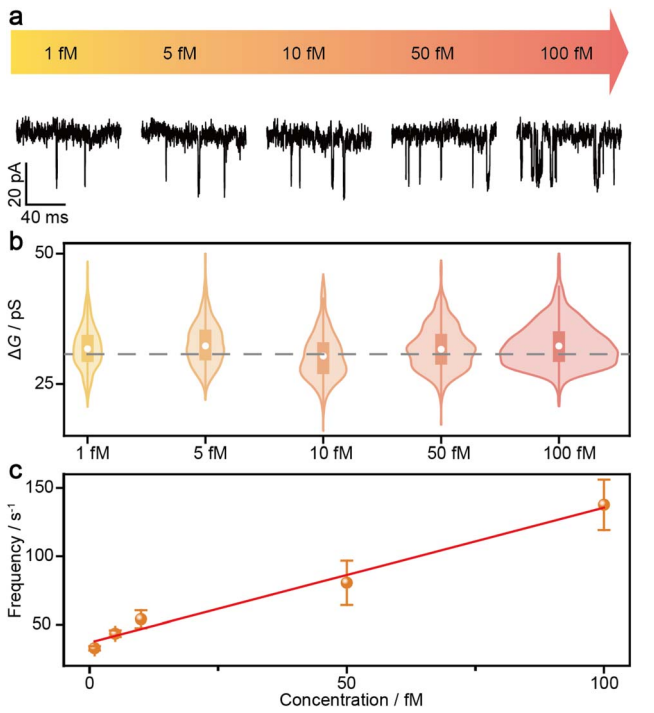

Fig. 3 Concentration-dependent event frequency with stable signal characteristics from 1 fM to 100 fM. (a) Current traces of GalA6 at sample concentrations from 1 fM to 100 fM in 0.2 M PB at pH 7.4 under 600 mV. (b) The violin plot of ΔG and GalA6 concentrations. White circles represent the same median of ΔG. (c) The event frequency was computed based on the number of events per unit time and directly proportional to sample concentrations from 1 fM to 100 fM.

To improve the accuracy and efficiency of oligosaccharide identification, a machine learning-based classifier model was used for autonomously analyzing single-molecule events. A database was built from six independent measurements of GalA-GalA6. Outliers beyond the 95% confidence interval were excluded to minimize data distortion, resulting in a final dataset of $N = 3600$. Using ΔG and dwell time as key features (ΔG contributing ~80% of predictive power, Fig. S16), the dataset was split into 80% for training and 20% for testing, with ten-fold cross-validation. Among the five evaluated classifiers, all achieved validation accuracy >0.92 with Random Forest performing best (0.97, Fig. 4a). Model performance stabilized with more than 535 training samples (Fig. S17 and S18). On the test set, it achieved 0.98 accuracy, misclassifying only 16/720 events (Fig. 4b). While some overlap between GalA3 and GalA4 was observed (Fig. S19), most species were well distinguished, demonstrating the model's utility for automated analysis of oligosaccharide samples.

To further assess the resolving power of nanopipettes in complex samples, mixtures of galacturonic acid oligosaccharides were analyzed. Oligosaccharides with one monosaccharide unit length difference were sequentially introduced into the cis chamber of the nanopipette at 10 fM for each species. The GalA/GalA2 mixture produced two distinct blockade types (Fig. 4c), with clear separation (separation ratio = 0.67, defined as the ratio of the peak-to-peak distance to the sum of their half-peak widths) confirmed by the scatter plot and Gaussian fitting (Fig. 4g). In mixtures, GalA2 exhibited prolonged dwell times, suggesting intermolecular interactions enhance differentiation. Similarly, GalA2/GalA3 and GalA5/GalA6 mixtures showed clear separation (separation ratios = 1.51 and 1.31; see details in SI Statistical Analysis), comparable to reported biological nanopores (0.46–3.11).[42] In the GalA2/GalA3 mixture, GalA2 exhibited a slight shift in ΔG and event duration (Fig. 4h), while GalA5/GalA6 mixtures revealed a noticeable increase in dwell time for GalA6 (Fig. 4i).

When all six oligosaccharides were mixed simultaneously, every species could be resolved (Fig. 4f). Their blockade profiles matched those obtained from pure samples (Fig. 4j). The Gaussian-fitted values of ΔG from Mono to Hexa were 28.9, 61.0, 99.6, 83.6, 18.3 and 38.2, with separation ratios of 1.43, 1.29, 0.61, 4.94 and 1.41. Using the established model, all types of events in a six-component mixture were successfully classified (Fig. S20). These findings demonstrate the capability of nanopipettes to discriminate galacturonic acid oligosaccharides at the single-molecule level, even in complex mixtures. To our knowledge, this is the first report of a solid-state nanopore capable of discriminating oligosaccharides differing in length by a single monosaccharide unit at the fM level.[43,44]

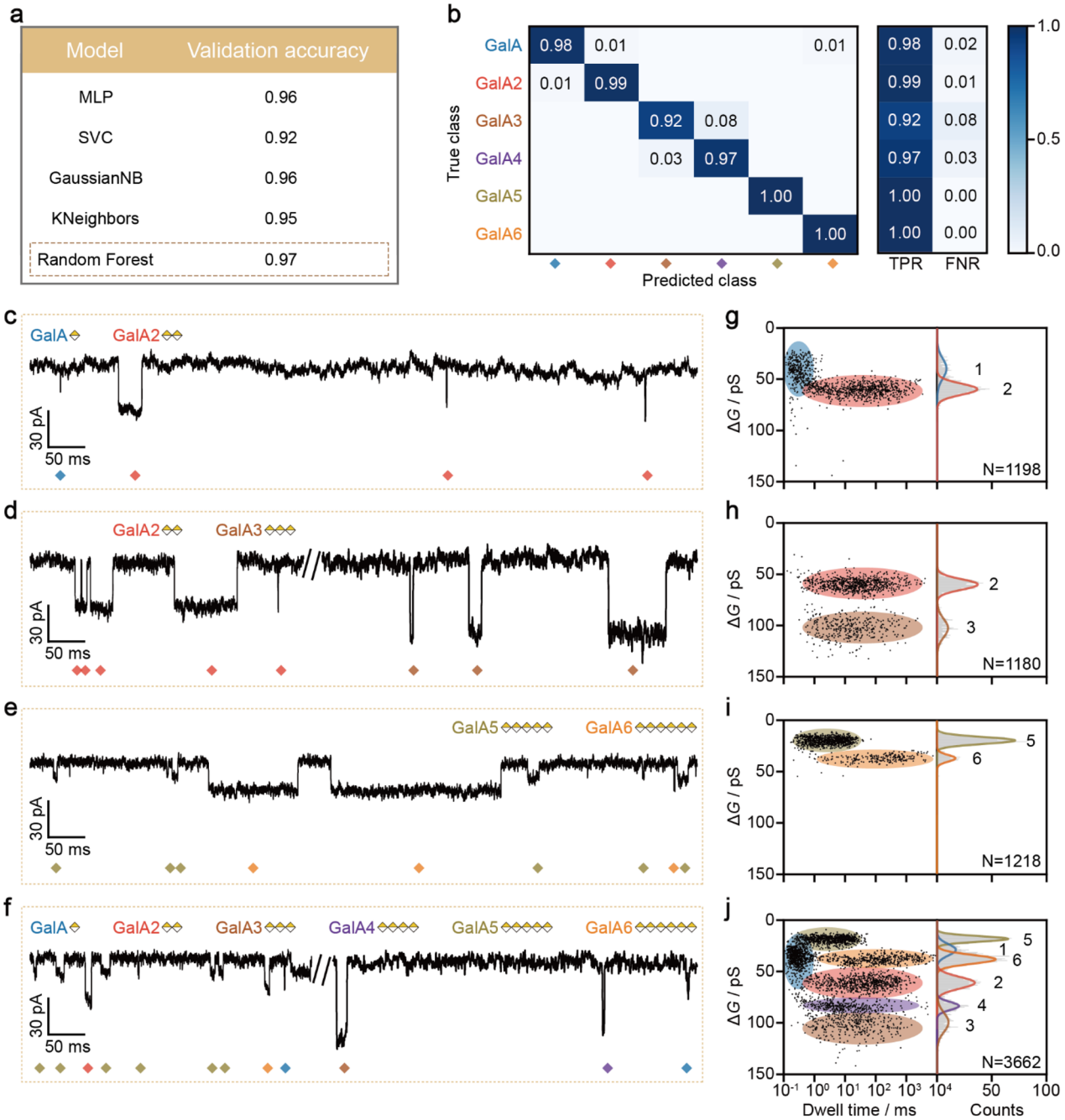

Fig. 4 Discrimination of oligosaccharide mixtures and machine learning of galacturonic acid oligosaccharides. (a) Performance assessment of different classification models. Five widely used models were trained and validated using 10-fold cross-validation. Among them, the Random Forest model demonstrated the highest accuracy, achieving a validation score of 0.97. (b) Confusion matrix for classification of galacturonic acid oligosaccharides using the Random Forest model. The true positive rate (TPR) and false negative rate (FNR) are displayed on the right. The overall classification accuracy reached 0.98, with accuracies of 1 achieved for GalA5 and GalA6. (c–f) Representative current traces for different oligosaccharide mixtures, with corresponding symbols on the left. Measurements were performed under identical conditions as individual analyte detections, with equimolar mixtures of GalA1-2, GalA2-3, GalA5-6, and GalA1-6. The final concentration of each oligosaccharide was maintained at 10 fM. Signal events were identified and marked with colored diamonds corresponding to each oligosaccharide. (g–j) Scatter plots and associated histogram curves of blockage events (bin size = 0.6) collected across mixture experiments. Numerical labels indicated the degree of polymerization of the galacturonic acid oligosaccharides corresponding to the fitted peaks.

Conclusions

In this study, we report the nanopipette capable of discriminating enzymatically derived oligosaccharides with single-monosaccharide length sensitivity at femtomolar concentrations. By integrating conductance blockade analysis with dwell time characterization, we were able to differentiate six enzymatically derived galacturonic acid oligosaccharides at the single-molecule level, both individually and in mixtures, with an accuracy of 0.98.

This study offers a potential nanopipette-based method for glycomics analysis, applicable to carbohydrate analysis in food science and biomedical diagnostics.[45,46] While the current work focuses on enzymatically derived oligosaccharides, the strategy can be extended to oligosaccharide products derived from alternative hydrolytic methods. Notably, our method achieves single-monosaccharide resolution for length discrimination. Crucially, it enables ultrasensitive detection at the femtomolar level. These two capabilities are hardly realized simultaneously in existing nanopore-based approaches (Table S4). Our study opens the possibility for detecting hydrolyzed oligosaccharides at physiologically relevant concentrations. Such capability could facilitate the analysis of oligosaccharides involved in gut microbiota metabolism such as real-time fermentation, thereby advancing the understanding of host–microbe interactions and prebiotic functionality. It could also enable sensitive analysis of plant-derived oligosaccharides, offering insights into their kinetic behavior during the enzymatic hydrolysis of cell wall polysaccharides, as well as their mechanisms of action as signaling molecules in regulating cellular chemical homeostasis to withstand external environmental perturbations. With further improvements in nanopore sensitivity (*e.g.*, *via* interfacial modification or the fabrication of smaller pore sizes), nanopipettes may ultimately enable low-concentration glycan sequencing.

Author contributions

H. M. and S. G. C. conceived the idea and designed the experiments. Q. Y. L. prepared the samples and conducted experiments on galacturonic acid oligosaccharides and analyzed the data. Q. Y. L. and H. M. prepared the figures and the manuscript draft. S. G. C. revised the manuscript. All authors discussed the results, provided input, and reviewed the manuscript at all stages.

Conflicts of interest

There are no conflicts to declare.

Data availability

The data that support the findings of this work have been included in the main text and supplementary information (SI). Supplementary information: supplementary methods, glycan characterization data, MS/MS spectra and nanopore characterization results. See DOI: https://doi.org/10.1039/d6sc00730a.

Acknowledgements

This research was supported by the "Pioneer" and "Leading Goose" R&D Program of Zhejiang (2025C01099), the National Natural Science Foundation of China (32250019), the Zhejiang University Global Partnership Fund (188170 + 194452506/011), and the Science Foundation of Zhejiang Sci-Tech University (24262198-Y). We acknowledge Professor Yi-Lun Ying from Nanjing University for providing the home-made nanopore instrument, data-processing software, and the insightful discussions on confined controlled electrochemistry.

Notes and references

1 J. Larsbrink, T. E. Rogers, G. R. Hemsworth, L. S. McKee, A. S. Tauzin, O. Spadiut, S. Klinter, N. A. Pudlo, K. Urs, N. M. Koropatkin, A. L. Creagh, C. A. Haynes, A. G. Kelly, S. N. Cederholm, G. J. Davies, E. C. Martens and H. Brumer, *Nature*, 2014, **506**, 498–502.
2 C. Reily, T. J. Stewart, M. B. Renfrow and J. Novak, *Nat. Rev. Nephrol.*, 2019, **15**, 346–366.
3 C. J. Gray, L. G. Migas, P. E. Barran, K. Pagel, P. H. Seeberger, C. E. Eyers, G. J. Boons, N. L. B. Pohl, I. Compagnon, G. Widmalm and S. L. Flitsch, *J. Am. Chem. Soc.*, 2019, **141**, 14463–14479.
4 C. Ferrara, S. Grau, C. Jäger, P. Sondermann, P. Brünker, I. Waldhauer, M. Hennig, A. Ruf, A. C. Rufer, M. Stihle, P. Umaña and J. Benz, *Proc. Natl. Acad. Sci. U. S. A*, 2011, **108**, 12669–12674.
5 M. J. Gnoth, S. Rudloff, C. Kunz and R. K. H. Kinne, *Food Res. Int.*, 2002, **35**, 145–149.
6 Q. Wu, Q. Wang, X. Luo, P. Jin, M. Jin, S. Hussain, Y. Qi, J. Mo, Y. Yu, H. Shao and L. Luo, *Nat. Commun.*, 2025, **16**, 6100.
7 B. S. Blaum, J. P. Hannan, A. P. Herbert, D. Kavanagh, D. Uhrín and T. Stehle, *Nat. Chem. Biol.*, 2015, **11**, 77–82.
8 C. Fontana and G. Widmalm, *Chem. Rev.*, 2023, **123**, 1040–1102.
9 J. Hofmann, H. S. Hahm, P. H. Seeberger and K. Pagel, *Nature*, 2015, **526**, 241–244.
10 M. Grabarics, M. Lettow, C. Kirschbaum, K. Greis, C. Manz and K. Pagel, *Chem. Rev.*, 2022, **122**, 7840–7908.
11 R. M. Gathungu, R. Kautz, B. S. Kristal, S. S. Bird and P. Vouros, *Mass Spectrom. Rev.*, 2020, **39**, 35–54.
12 K. Zhu, J. Wu, A. Hu, Z. Yin, Z. Hou, X. Ye and S. Chen, *J. Agric. Food Chem.*, 2024, **72**, 9117–9127.
13 J. Helm, C. Grünwald-Gruber, A. Thader, J. Urteil, J. Führer, D. Stenitzer, D. Maresch, L. Neumann, M. Pabst and F. Altmann, *Anal. Chem.*, 2021, **93**, 15175–15182.
14 A. L. Marie, Y. Gao and A. R. Ivanov, *Nat. Commun.*, 2024, **15**, 3847.
15 S. Howorka and Z. Siwy, *Chem. Soc. Rev.*, 2009, **38**, 2360–2384.
16 P. Bayat, C. Rambaud, B. Priem, M. Bourderioux, M. Bilong, S. Poyer, M. Pastoriza-Gallego, A. Oukhaled, J. Mathé and R. Daniel, *Nat. Commun.*, 2022, **13**, 5113.

17 B. Xia, J. Fang, S. Ma, M. Ma, G. Yao, T. Li, X. Cheng, L. Wen and Z. Gao, *J. Am. Chem. Soc.*, 2023, **145**, 18812–18824.
18 F. Gao, J. Wang, H. Ma, B. Xia, L. Wen, Y. Long and Y. Ying, *Angew. Chem., Int. Ed.*, 2025, **64**, e202422118.
19 W. J. Ramsay and H. Bayley, *Angew. Chem., Int. Ed.*, 2018, **57**, 2841–2845.
20 S. Zhang, Z. Cao, P. Fan, Y. Wang, W. Jia, L. Wang, K. Wang, Y. Liu, X. Du, C. Hu, P. Zhang, H. Chen and S. Huang, *Angew. Chem., Int. Ed.*, 2022, **61**, e202203769.
21 W. Lu, X. Zhao, M. Li, Y. Li, C. Zhang, Y. Xiong, J. Li, H. Zhou, X. Ye, X. Li, J. Wang, X. Liang and G. Qing, *ACS Nano*, 2024, **18**, 12412–12426.
22 Y. Zhang, A. Rana, Y. Stratton, M. F. Czyzyk-Krzeska and L. Esfandiari, *Anal. Chem.*, 2017, **89**, 9201–9208.
23 W. Xie, S. He, S. Fang, L. Liang, R. Tian and D. Wang, *Nanoscale*, 2023, **15**, 7147–7153.
24 R. Ren, S. Cai, X. Fang, X. Wang, Z. Zhang, M. Damiani, C. Hudlerova, A. Rosa, J. Hope, N. J. Cook, P. Gorelkin, A. Erofeev, P. Novak, A. Badhan, M. Crone, P. Freemont, G. P. Taylor, L. Tang, C. Edwards, A. Shevchuk, P. Cherepanov, Z. Luo, W. Tan, Y. Korchev, A. P. Ivanov and J. B. Edel, *Nat. Commun.*, 2023, **14**, 7362.
25 R. Zhu, F. Qin, X. Zheng, S. Fang, J. Ding, D. Wang and L. Liang, *Biosens. Bioelectron.*, 2023, **240**, 115641.
26 L. Guo, Y. Han, H. Yang, J. Fu, W. Li, R. Xie, Y. Zhang, K. Wang and X. H. Xia, *Nano Lett.*, 2024, **24**, 5639–5646.
27 J. Im, S. Lindsay, X. Wang and P. Zhang, *ACS Nano*, 2019, **13**, 6308–6318.
28 B. I. Karawdeniya, Y. M. N. D. Y. Bandara, J. W. Nichols, R. B. Chevalier and J. R. Dwyer, *Nat. Commun.*, 2018, **9**, 3278.
29 Y. Sun, Z. Mi, X. Chen, J.-J. Li, J. Lu, X. Shan, X. Lu and Y. Du, *Sci. Rep.*, 2024, **14**, 32000.
30 F. Rivas, P. L. DeAngelis, E. Rahbar and A. R. Hall, *Sci. Rep.*, 2022, **12**, 4469.
31 A. G. Jimenez, M. Ellermann, W. Abbott and V. Sperandio, *Nat. Microbiol.*, 2020, **5**, 368–378.
32 W. Tang, T. Han, W. Liu, J. He and J. Liu, *Crit. Rev. Food Sci. Nutr.*, 2024, 1–17.
33 A. Hosseini-Abari, G. Emtiazi, M. Jazini, J. Kim and B. G. Kim, *J. Basic Microbiol.*, 2019, **59**, 249–255.
34 H. Y. Y. Yao, J. Q. Wang, J. Y. Yin, S. P. Nie and M. Y. Xie, *Food Res. Int.*, 2021, **143**, 110290.
35 M. E. Cano, A. García-Martín, M. Ladero, D. Lesur, S. Pilard and J. Kovensky, *Food Chem.*, 2021, **346**, 128909.
36 S. Turella, C. He, L. Zhao, S. Banerjee, L. Plouhinec, R. Assiah Yao, M. C. Nørgaard Kejlstrup, S. Grisel, Y. So, B. Annic, M. Fanuel, M. Haddad Momeni, B. Bissaro, S. Meier, J. P. Morth, S. Dong, J.-G. Berrin and M. Abou Hachem, *Nat. Commun.*, 2025, **16**, 3467.
37 J. Ritmejeris, X. Chen and C. Dekker, *Nat. Rev. Bioeng.*, 2024, **3**, 303–316.
38 Y. L. Ying, Z. L. Hu, S. Zhang, Y. Qing, A. Fragasso, G. Maglia, A. Meller, H. Bayley, C. Dekker and Y.-T. Long, *Nat. Nanotechnol.*, 2022, **17**, 1136–1146.
39 S. Ferrari, D. V. Savatin, F. Sicilia, G. Gramegna, F. Cervone and G. D. Lorenzo, *Front. Plant Sci.*, 2013, **4**, 49.
40 K. J. Freedman, L. M. Otto, A. P. Ivanov, A. Barik, S.-H. Oh and J. B. Edel, *Nat. Commun.*, 2016, **7**, 10217.
41 R. Nouri, Z. Tang and W. Guan, *ACS Sens.*, 2019, **4**, 3007–3013.
42 G. Yao, B. Xia, F. Wei, J. Wang, Y. Yang, S. Ma, W. Ke, T. Li, X. cheng, L. Wen, Y. Long and Z. Gao, *J. Am. Chem. Soc.*, 2025, **147**, 1721–1731.
43 Y. Cai, B. Zhang, L. Liang, S. Wang, L. Zhang, L. Wang, H. L. Cui, Y. Zhou and D. Wang, *Plant Commun.*, 2021, **2**, 100106.
44 K. Xia, J. T. Hagan, L. Fu, B. S. Sheetz, S. Bhattacharya, F. Zhang, J. R. Dwyer and R. J. Linhardt, *Proc. Natl. Acad. Sci. U. S. A*, 2021, **118**, e2022806118.
45 W. Tang, D. Liu and S. P. Nie, *Curr. Opin. Food Sci.*, 2022, **46**, 100850.
46 G. Yao, W. Ke, B. Xia and Z. Gao, *Chem. Sci.*, 2024, **15**, 6229–6243.